11.2A Examining the sensitivities of high-shear, low-CAPE convection to low-level hodograph shape

Keith D. Sherburn* and Matthew D. Parker
Department of Marine, Earth, and Atmospheric Sciences, North Carolina State University, Raleigh, North Carolina

1. Introduction

Overnight and cool season convection capable of producing severe hazards in the Southeast, Ohio Valley, and Mississippi Valley often occurs in environments characterized by intense synoptic-scale forcing and kinematics but weak buoyancy (e.g., Schneider et al. 2006; Clark 2009; Guyer and Dean 2010; Sherburn and Parker 2014a). These high-shear, low-CAPE (HSLC) environments represent a considerable challenge to operational forecasters due to their associated low probability of detection and high false alarm rates with severe weather watches and warnings (e.g., Dean et al., 2009; Davis and Parker 2014). Typically, HSLC environments are considered to be those falling within a parameter space of surface-based (SB) or mixed-layer (ML) CAPE ≤ 500 to 1000 J kg^{-1} and deep-layer shear vector magnitude ≥ 18 m s^{-1} (e.g., Schneider et al. 2006; Guyer and Dean 2010; Sherburn and Parker 2014a). The reader is directed to Sherburn and Parker (2014b) for a more detailed background on HSLC environments and their associated severe hazards.

Though shear vector *magnitude* is often utilized independently as an operational guidance parameter (such as in the HSLC criteria defined above), the shear vector *orientation*, particularly that relative to synoptic-scale and mesoscale boundaries, has been shown in previous studies to play a significant role in the evolution of convection (Bluestein and Weisman 2000; French and Parker 2008; Dial et al. 2010). The aforementioned studies show that the component of the deep-layer shear vector normal to forcing usually dictates the resulting convective mode and associated hazards. Similarly, several studies have noted that the shear vector magnitude over shallower layers (e.g., 0-0.5 km, 0-1 km, 0-3 km), especially that relative to system-generated cold pools, influences the potential development, strengthening, and maintenance of low-level vortices in supercells and QLCSs (Brooks et al. 2003; Markowski et al. 2003; Weisman and Trapp 2003; Atkins and St. Laurent 2009; Schaumann and Przybylinski 2012; Coffer and Parker 2015).

HSLC environments intrinsically lack substantial buoyancy; thus, to produce significantly severe hazards, this marginal buoyancy must be compensated by strong synoptic-scale and mesoscale forcing and, on the storm scale, dynamic forcing via the updraft-in-shear effect and the vertical perturbation pressure gradient acceleration in rotating updrafts. Synoptic-scale and mesoscale forcing is often provided by progressive cold fronts. The strength and orientation of flow relative to these boundaries is expected to play a significant role in subsequent convective evolution, perhaps more so than in setups with higher ambient buoyancy. To this end, in comparing high-impact HSLC severe convective events across the southeastern U.S., Sherburn (2013) found that events associated with a relatively large number of tornadoes (i.e., ≥ 20) were characterized by larger cross-boundary components of the wind and shear vectors than those associated with primarily or entirely straight-line severe winds, while the latter cases had smaller cross-boundary components of wind and shear vectors and larger along-boundary components. Further, although dynamic forcing for ascent on the storm scale is largely dependent on shear vector magnitude (e.g., Weisman and Rotunno 2000), the orientation of low-level and deep-layer shear vectors may be underestimated, especially in HSLC environments. However, despite reasonable assertions and cursory exploration, sensitivities to the shape and orientation of the hodograph in HSLC environments remain largely unexplored and, consequently, poorly understood.

Ultimately, through this and a series of future sensitivity studies, we seek to fill the general knowledge gap associated with severe HSLC convection. This study, the first in the series, will allow for a more thorough understanding of how the low-level kinematic profile influences the lifecycle and potential severity of HSLC convection—including its development, evolution,

**Corresponding author address*: Keith Sherburn, Department of Marine, Earth, and Atmospheric Sciences, Campus Box 8208, North Carolina State University, Raleigh, NC 27695-8208

and potential for producing strong, long-lived, near-surface vortices—to variability in low-level hodograph shape and orientation. Our focus here will be entirely on the hodograph in the lowest km, as preliminary numerical investigations revealed that the 0-1 km shear vector magnitude was strongly correlated with the potential of producing intense near-surface vortices.

2. Methods

A matrix of 12 idealized simulations was developed by using four control hodographs ("L-shaped", "Ball cap", "Quarter turn", and "Spatula") and rotating each 45° counterclockwise (CCW) and clockwise (CW), as shown in Figure 1. The resulting profiles showed several similarities to those generated by compositing cases associated with HSLC severe convection (cf. Figs. 1, 2). All simulations had identical, homogeneous thermodynamic profiles approximately representative of a "high-end" HSLC thermodynamic environment (Fig. 3). Bulk wind differences (BWDs) in the 0-1 km (25 m s^{-1}), 0-3 km (30 m s^{-1}), and 0-6 km (40 m s^{-1}) layers were identical in each simulation. Thus, the only variability was in the 0-1 km hodograph shape and the wind profile orientation. Shear vector magnitudes, similar to the amount of 0-3 km CAPE exhibited in the thermodynamic profile, lie at the upper end of the observed range within HSLC severe events.

Simulations were performed with the Bryan Cloud Model (CM1; Bryan and Fritsch 2002) and initialized with a 2.5-km deep, north-south oriented cold pool consisting of minimum potential perturbations of -6 K and a prescribed initial difference in zonal winds (relative to the ambient environment) of 20 m s^{-1}. Horizontal grid spacing was 250 m, with the x-domain stretched outside of the inner 100 km to lower the computational demand. The vertical grid was stretched from 100 m at the lowest model level (50 m) to 500 m from 6 km to the top of the domain. Boundaries were open in the x-direction and periodic in the y-direction, while surface fluxes and Coriolis forcing were neglected. The NSSL 2-moment microphysics scheme including graupel and hail was utilized, and minor initial random potential temperature perturbations were included across the domain to encourage more rapid three-dimensional evolution of convection. Simulations were run for a period of 5 h.

Additionally, cursory investigations varying grid resolution, microphysics schemes, initiation mechanism, and initial convergence along the cold pool leading edge were undertaken. Brief remarks about these studies will be provided in the following section.

3. Results

Several behaviors were observed across the matrix of simulations, though not all were representative of typical HSLC severe convection. For clarity and brevity within this work, we chose to focus on the four most realistic and intense simulations.

a. The four core simulations

Four simulations—the control L-shaped, the CCW ball cap, the control quarter turn, and the control spatula—represent the "core" simulations referred to here. These simulations showed strong and realistic but varying solutions, allowing for a reasonably contained investigation into the influence of low-level hodograph shape and orientation on subsequent convective evolution. The characteristics of these simulations will be explored in turn.

i. L-shaped control

The L-shaped control hodograph contains entirely boundary-parallel flow in the lowest 1 km, with increasingly cross-boundary flow above 1 km. Convection in this environment remains tied to the initiating boundary (see Fig. 4). Early in the simulation, updrafts are primarily linear, with similarly linear reflectivity signatures. Over time, embedded bowing segments and supercellular features emerge. Despite updrafts stronger than 10 m s^{-1} over a depth of more than 7 km (the deepest of any simulation), any near-surface vortex that develops remains weak compared to other simulations, with values remaining below 0.05 s^{-1}. This is true even for vortices exhibiting vertical continuity from the surface to mid-levels, as shown in Figure 5. The lack of intensification is likely due to the strong negative buoyancy associated with the near-surface vortices in this simulation, similar to the strong low-level shear and strong heat sink case presented by Markowski and Richardson (2014).

This simulation implies that boundary-relative flow in even the lowest 1 km is critical in determining whether or not convection will remain tied to the boundary. This has significant ramifications for the potential for producing intense near-surface vortices. Despite a lack of significant low-level vortices in the L-shaped control simulation, the updrafts were of comparable strength and greater depth than the other three core simulations. This can likely be attributed to the large amount of low-level streamwise vorticity contributed by both the ambient flow and the added eastward push from the initiating boundary.

ii. Ball cap CCW

The CCW ball cap hodograph closely resembles the composite non-supercell hodograph from Sherburn (2013; cf. Figs. 1 and 2). The morphology of simulated convection here is consistent with those composites, as convection has generally linear characteristics, though occasional, transient rotating updrafts are observed (Fig. 6). Ultimately, this simulation produces primarily linear updraft structures—similar to the L-shaped case—but only a moderate cold pool, the latter feature perhaps contributing to the strong, long-lived vortices observed in this simulation. Reflectivity structures are also more aligned with the initial boundary than in the quarter-turn simulation to be discussed shortly, likely due to the stronger line-parallel flow above 1 km. This leads to closer proximity of downdrafts and updrafts of adjacent cells, the potential ramifications of which are explored in the next section.

iii. Quarter turn control and spatula control

Whereas the ball cap CCW hodograph is similar to the composite *non*-supercell hodograph from Sherburn (2013), the quarter turn control hodograph resembles the composite *supercell* hodograph (cf. Figs. 1 and 2). While the updrafts in this simulation are not the deepest, they are the strongest and exhibit mid-level rotation more persistently than the other core simulations (Fig. 7). Despite the subtle differences in hodograph structure in the lowest 1 km between the quarter turn control and spatula control simulations, resulting convective strength and production of low-level vortices is remarkably dissimilar (cf. Figs. 7 and 8).

In particular, the quarter turn control simulation produces the most intense near-surface vortices of all simulations, with vertical vorticity values at the lowest model level exceeding 0.15 s^{-1} (Figs. 5 and 9). Some of these occur within the first two hours of the simulation; on the contrary, the strongest near-surface vortices in the spatula control simulation remain below 0.1 s^{-1} and occur after 160 min. Additionally, updrafts, mid-level rotation, and cold pool potential temperature perturbation are noticeably weaker in the spatula control run, especially within the first 2.5 h.

Streamwise vorticity in shallow layers near the ground appears to be the primary difference between the quarter turn control and spatula control simulations. Because the 0-1 km, 0-3 km, and 0-6 km shear vectors are identical across the two environments, the sole discriminating factor is the curvature in the lowest 1 km of the quarter turn hodograph. This leads to an enhancement of streamwise vorticity in the quarter turn simulation, particularly in the lowest 0.5 km. The mechanisms relating increased low-level streamwise vorticity to an enhancement of low-level vortex strength will be a focus of future work, though we speculate they may be similar to the lowering of strong dynamic forcing for ascent via the upward-directed perturbation pressure gradient acceleration discussed by Coffer and Parker (2015).

Comparing the ball cap CCW and quarter turn control hodographs, the primary differences are above 1 km. It appears that one role of the flow in the mid and upper levels is to affect precipitation fallout, ultimately providing the varying reflectivity structures observed in these two cases. Increased line-parallel flow leads to decreased spacing between updrafts and adjacent cells' downdrafts, resulting in more unsteadiness in near-surface vertical vorticity centers. This ultimately leads to weaker vortices in the ball cap CCW simulation when compared to the quarter turn control simulation, though some still become quite intense and long-lived. More quantitative analysis is necessary to confirm these ideas

b. Additional matrix simulations

Across the eight other simulations, three primary behaviors were observed: a) overrunning convection, when low- and mid-level flow was largely parallel to or atop the initial boundary (Fig. 10), b) shear-parallel convective bands, when low- and mid-level flow was largely perpendicular to the initial boundary, allowing for self-organization of convection (Fig. 11), and c) realistic-looking convection that was either weaker or less representative than the four core simulations. These simulations will not be investigated further here but may be a subject of future detailed analysis.

c. Additional sensitivity studies

Less formal sensitivity studies were conducted to investigate the influences of grid resolution, idealized initiation mechanism, and initial prescribed convergence along the cold pool leading edge. While these have yet to be subject to rigorous quantitative assessment, some preliminary findings include:

- Convection is poorly defined at grid spacings of 0.5 km and 1 km, though general structures are marginally resolved. At grid spacings larger than 1 km, convection is very weak and short-lived.
- Initial triggers other than a cold block (including a single warm bubble, a line of warm bubbles, a line thermal, and a zone of constant convergence) are unable to produce sustained HSLC convection.
- Although convective trends and behaviors were similar, convection was *typically* weaker when initial convergence at the cold pool leading edge was weaker.

4. Conclusions

Cognizant of the role of linear forcing for ascent in the development and evolution of HSLC convection, this study focused on varying the base-state hodograph shape in the lowest 1 km and orientation of the wind profile relative to an initial cold block to determine the resultant impact on convective characteristics. As expected, the matrix of 12 simulations revealed a variety of convective behaviors, including realistic QLCSs with occasional embedded supercells, overrunning convection, and shear-parallel convective bands. Further analysis is required to entirely explain the observed differences, but some preliminary conclusions include:

- Streamwise vorticity in the lowest levels (e.g., 0-1 km or 0-0.5 km) appears critical for the development of strong, rotating updrafts in HSLC environments and could be one of the discriminating factors in whether or not intense near-surface vortices will be produced.
- Boundary-relative flow in the lowest 1 km affects convection's ability to move off of an initial boundary. More cross-boundary flow appears to result in convection moving off the boundary, potentially becoming discrete or organizing into shear-parallel bands, while along-boundary flow promotes linear updrafts.
- HSLC convection tied to a strong boundary may struggle to produce intense, long-lived near-surface vortices, likely due to strong negative buoyancy associated with the cold pool.
- Mid- and upper-level flow plays a role in precipitation fallout, which may affect the proximity of updrafts and downdrafts of adjacent cells. This *could* play a role in the disruption (or lack thereof) of vortex genesis or maintenance.
- Operational meteorologists must investigate the hodograph, especially in the lowest levels, to accurately determine the potential for HSLC convection to produce intense near-surface vortices. Shear vector orientation and magnitude alone are insufficient. Care must be taken to also consider the strength and motion of initiating boundaries.

Future work will explore the development, strengthening, and maintenance of low- and mid-level vortices, including their failure points. Additionally, we would like to investigate the origins of low-level rotation and compare those to studies of supercells in high-CAPE environments (e.g., Dahl et al. 2014). We also plan to explore additional sensitivity tests, such as varying the relative humidity and depth of buoyancy in the initial thermodynamic profile, the strength of linear forcing, and the orientation of deeper layers of shear. Finally, we acknowledge that HSLC events in particular are not independent of environmental heterogeneity. To address this, real-case simulations nested to fine grid resolutions are necessary to determine the mesoscale and synoptic scale influences on storm-scale processes within HSLC environments, such as undertaken by King and Parker (2014, 2015).

REFERENCES

Atkins, N. T., and M. St. Laurent, 2009: Bow Echo Mesovortices. Part II: Their Genesis. *Mon. Wea. Rev.*, **137**, 1514-1532.

Bluestein, H. B., and M. L. Weisman, 2000: The interaction of numerically simulated supercells initiated along lines. *Mon. Wea. Rev.,* **128**, 3128-3149.

Brooks, H. E., J. W. Lee, and J. P. Craven, 2003: The spatial distribution of severe thunderstorm and tornado environments from global reanalysis data. *Atmos. Res.*, **67-68**, 73-94.

Bryan, G. H., and J. M. Fritsch, 2002: A benchmark simulation for moist nonhydrostatic numerical models. *Mon. Wea. Rev.*, **130**, 2917-2928.

Clark, M. R., 2009: The southern England tornadoes of 30 December 2006: Case study of a tornadic storm in a low CAPE, high shear environment. *J. Atmos. Res.,* **93**, 50-65.

Coffer, B. E., and M. D. Parker, 2015: Impacts of increasing low-level shear on supercells during the early evening transition. *Mon. Wea. Rev.*, **143**, 1945-1969.

Dahl, J. M. L., M. D. Parker, L. J. Wicker, 2014: Imported and storm-generated near-ground vertical vorticity in a simulated supercell. *J. Atmos. Sci.*, **71**, 3027-3051.

Davis, J. M., and M. D. Parker, 2014: Radar climatology of tornadic and non-tornadic vortices in high shear, low CAPE environments in the mid-Atlantic and southeastern U.S. *Wea. Forecasting*, **29**, 828-853.

Dean, A. R., R. S. Schneider, R. L. Thompson, J. A. Hart, and P. D. Bothwell, 2009: The conditional risk of severe convection estimated from NWS Storm Prediction Center mesoscale objective analyses: Potential uses in support of forecast operations and verification. Preprints, *23rd Conf. on Weather Analysis and Forecasting*, Omaha, NE, 6A.5.

Dial, G. L., J. P. Racy, and R. L. Thompson, 2010: Short-term convective mode evolution along synoptic boundaries. *Wea. Forecasting*, **25**, 1430-1446.

French, A. J., and M. D. Parker, 2008: The initiation and evolution of multiple modes of convection within a meso-alpha scale region. *Wea. Forecasting,* **23**, 1221-1252.

Guyer, J. L., and A. R. Dean, 2010: Tornadoes within weak CAPE environments across the continental United States. Preprints, *25th AMS Conf. on Severe Local Storms*, Denver, CO, AMS, 1.5.

King, J. R., and M. D. Parker, 2014: Synoptic influence on high shear, low CAPE convective events. Preprints, *27th Conf. on Severe Local Storms*, Madison, WI, AMS, P59.

King, J. R., and M. D. Parker, 2015: Conditioning and evolution of high shear, low CAPE environments. Preprints, *16th Conf. on Mesoscale Processes*, Boston, MA, AMS, 12.5.

Markowski, P. M., and Y. P. Richardson, 2014: The influence of environmental low-level shear and cold pools on tornadogenesis: Insights from idealized simulations. *J. Atmos. Sci.*, **71**, 243-275.

Markowski, P. M., C. Hannon, J. Frame, E. Lancaster, A. Pietrycha, R. Edwards, and R. L. Thompson, 2003: Characteristics of vertical wind profiles near supercells obtained from the Rapid Update Cycle. *Wea. Forecasting*, **18**, 1262-1272.

Schaumann, J. S., and R. W. Przybylinski, 2012: Operational application of 0-3 km bulk shear vectors in assessing QLCS mesovortex and tornado potential. Preprints, *26th Conf. on Severe Local Storms*, Nashville, TN, AMS, P9.10.

Schneider, R. S., A. R. Dean, S. J. Weiss, and P. D. Bothwell, 2006: Analysis of estimated environments for 2004 and 2005 severe convective storm reports. Preprints, *24th Conf. on Severe Local Storms*, St. Louis, MO, AMS.

Sherburn, K. D., 2013: Improving the Understanding and Forecasting of Severe High Shear, Low CAPE Environments. M.S. thesis, Dept. of Marine, Earth, and Atmospheric Sciences, North Carolina State University, 124 pp. [Available online at: http://repository.lib.ncsu.edu/ir/bitstream/1840.16/8666/1/etd.pdf]

Sherburn, K. D., and M. D. Parker, 2014a: Climatology and ingredients of significant severe convection in high-shear, low-CAPE environments. *Wea. Forecasting*, **29**, 854-877.

Sherburn, K. D., and M. D. Parker, 2014b: High-shear, low-CAPE environments: What we know and where to go next. Preprints, *27th Conf. on Severe Local Storms*, Portland, OR, AMS, 12B.2.

Weisman, M. L., and R. Rotunno, 2000: The use of vertical wind shear versus helicity in interpreting supercell dynamics. *J. Atmos. Sci.*, **57**, 1452-1472.

Weisman, M. L., and R. J. Trapp, 2003: Low-level mesovortices within squall lines and bow echoes. Part I: Overview and dependence on environmental shear. *Mon. Wea. Rev.*, **131**, 2779-2803.

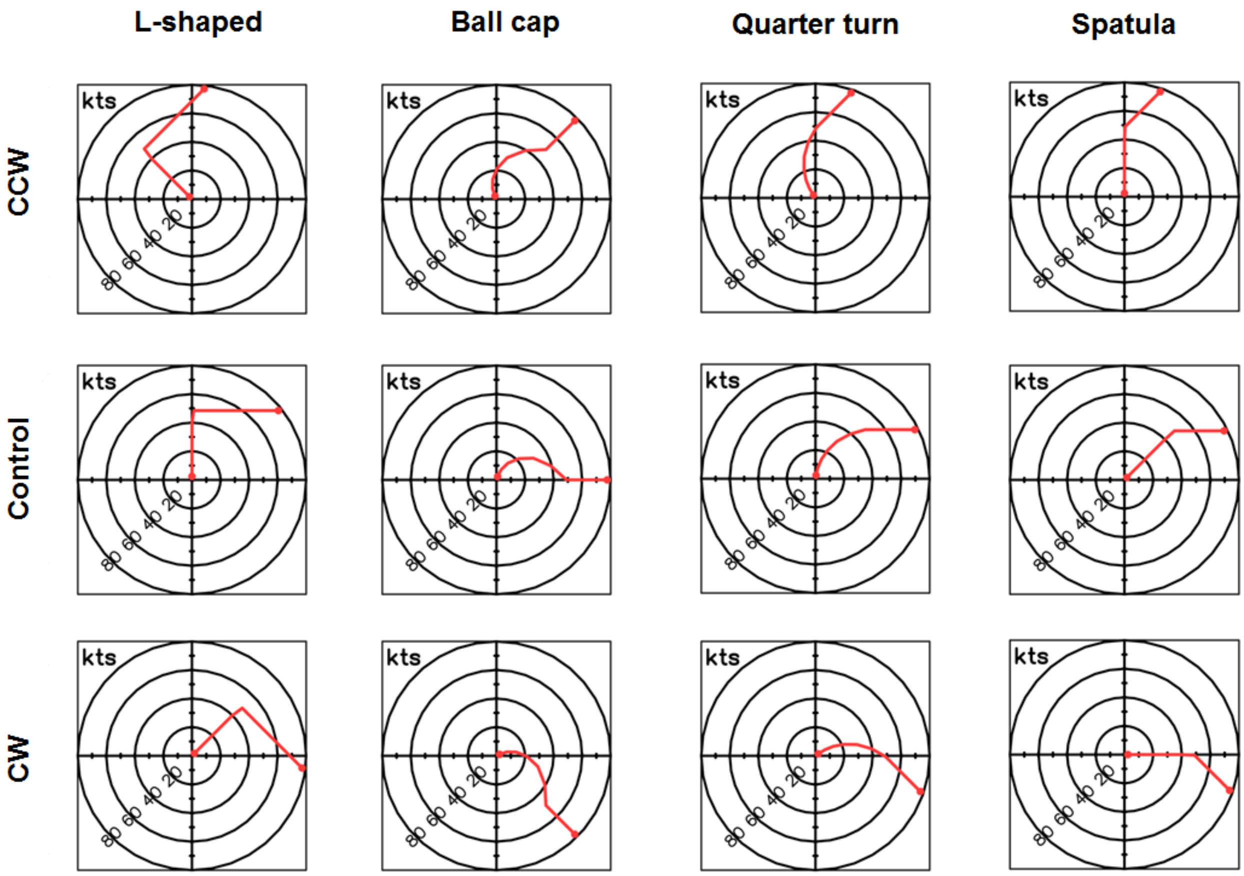

Figure 1. Matrix of 12 hodographs utilized in this study. Four control hodographs are rotated 45° counterclockwise (CCW) and clockwise (CW) to achieve the matrix of 12.

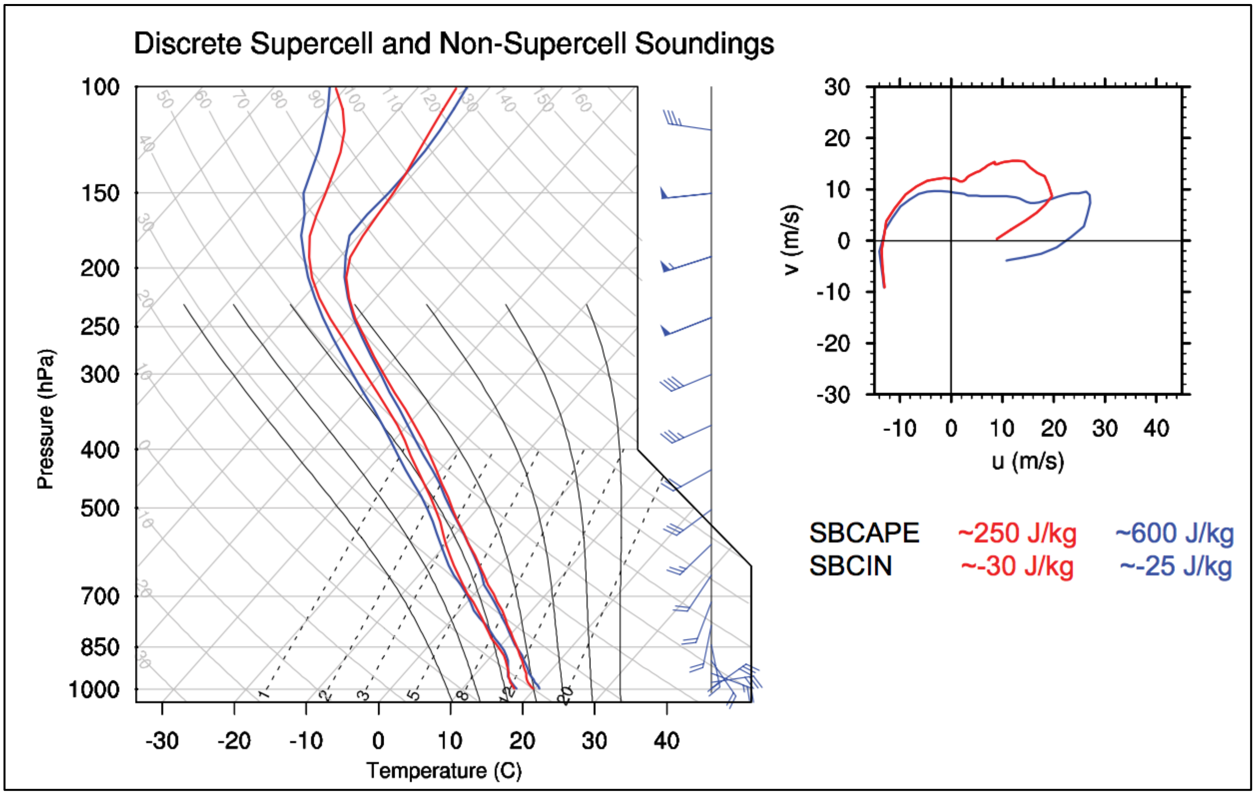

Figure 2. Composite soundings representing HSLC environments producing severe discrete supercells (blue) and non-supercells (red) generated from archived Rapid Update Cycle (RUC) analyses.

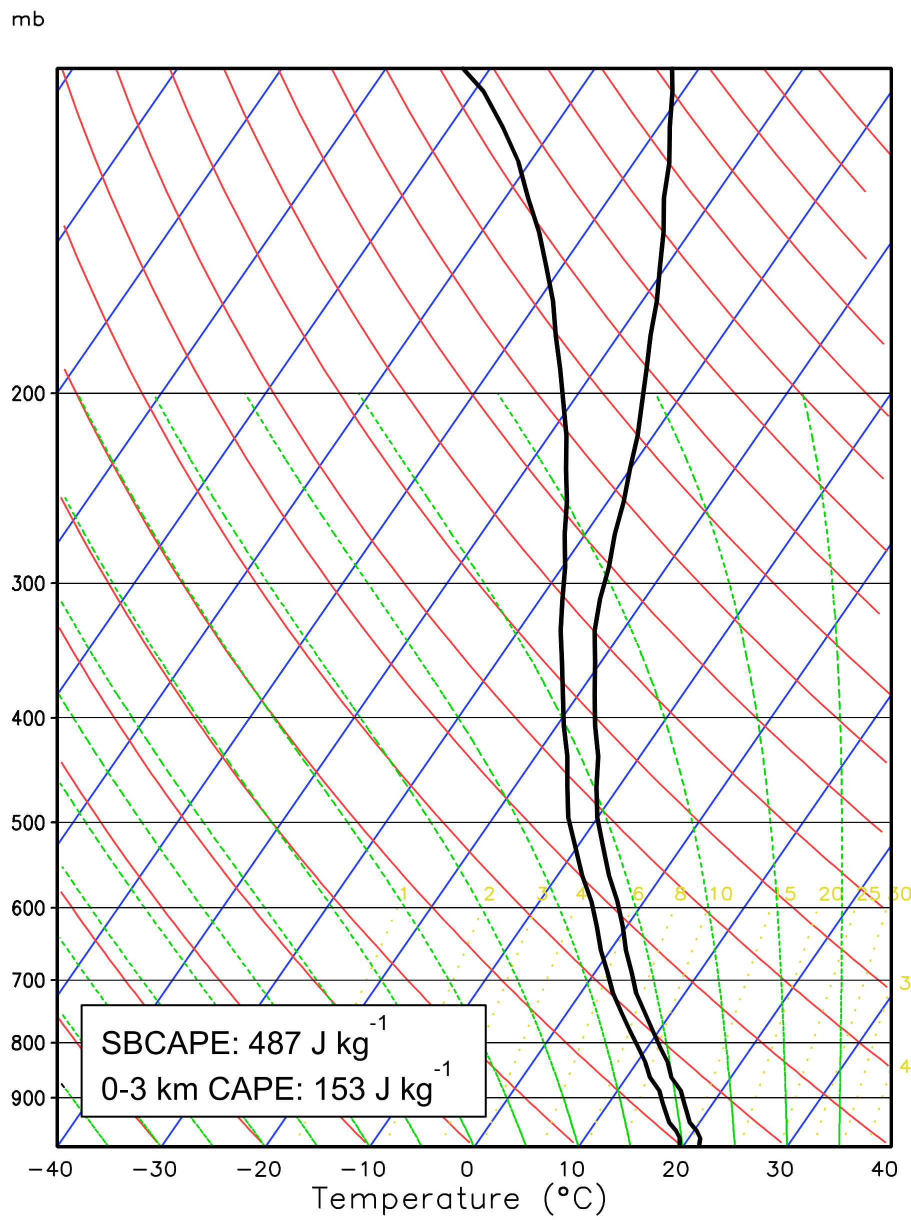

Figure 3. Thermodynamic profile utilized in the matrix of 12 simulations. Inset shows the associated surface-based CAPE (SBCAPE) and 0-3 km CAPE.

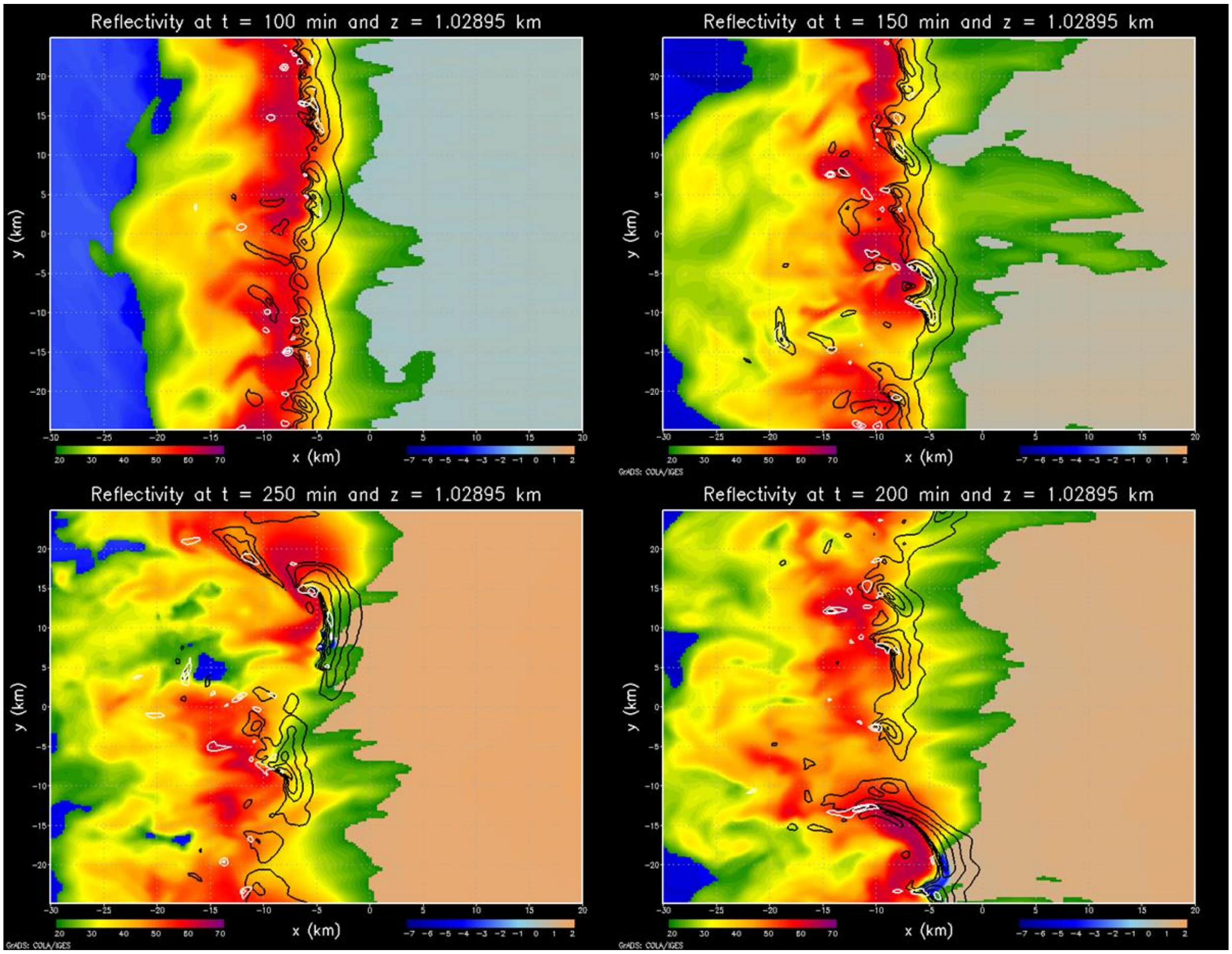

Figure 4. 1-km simulated radar reflectivity (dBZ; green through purple shading), lowest level θ' (K, blue to tan shading), 1-km vertical velocity (black contours at 2.5, 5, 7.5, 10, 15, and 20 m s^{-1}), and 1-km vertical vorticity (white contours at 0.01 s^{-1} intervals from 0.01 s^{-1} to 0.1 s^{-1}) for L-shaped control simulation at (clockwise, from top left) t = 100 min, 150 min, 200 min, and 250 min.

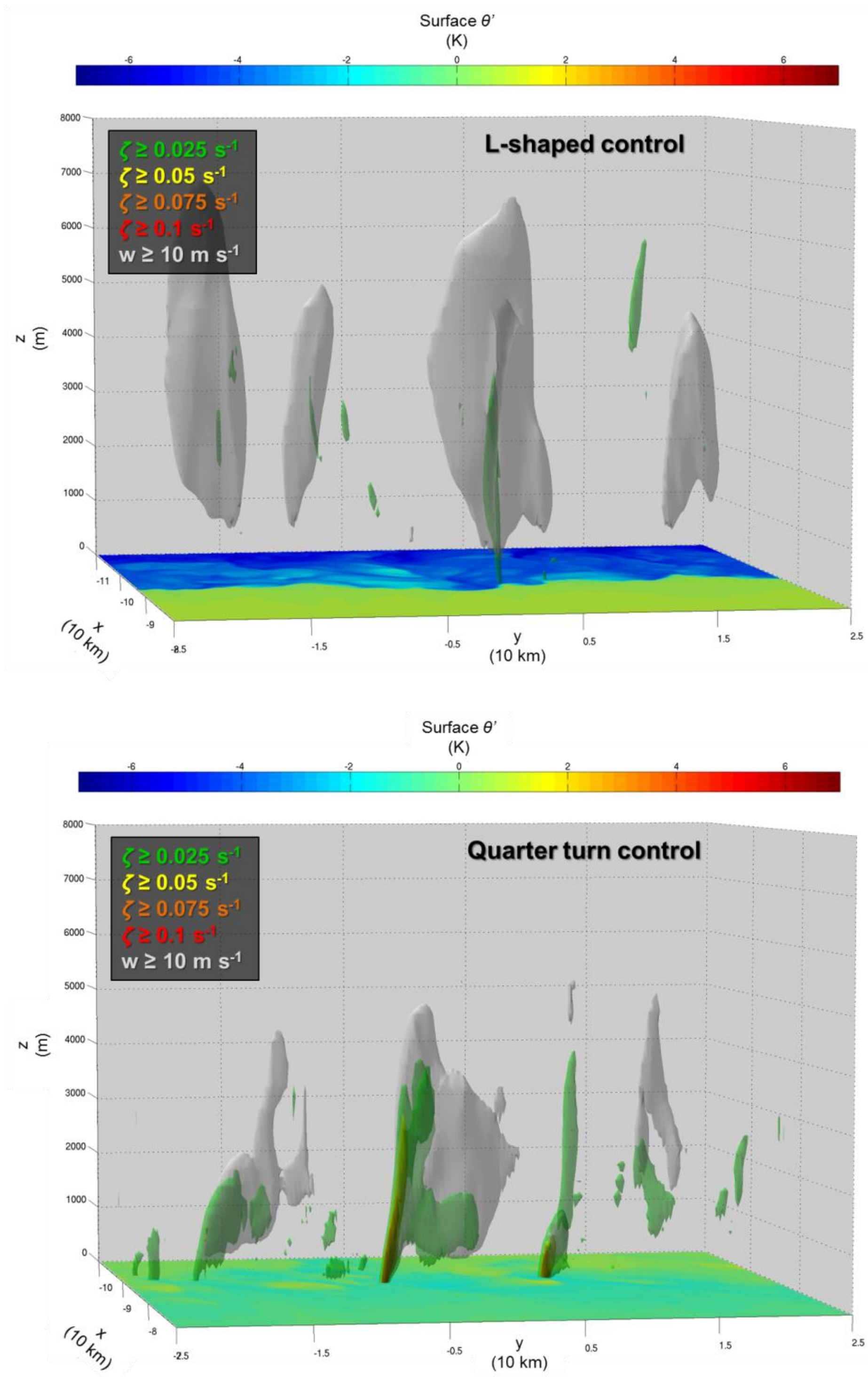

Figure 5. 3D isosurfaces of vertical velocity (grey, at least 10 m s^{-1}) and vertical vorticity (as labeled) with surface θ' shaded on the ground for the L-shaped control and quarter turn control simulations. Note the deeper updrafts, colder θ', and weaker vortices in the L-shaped control run.

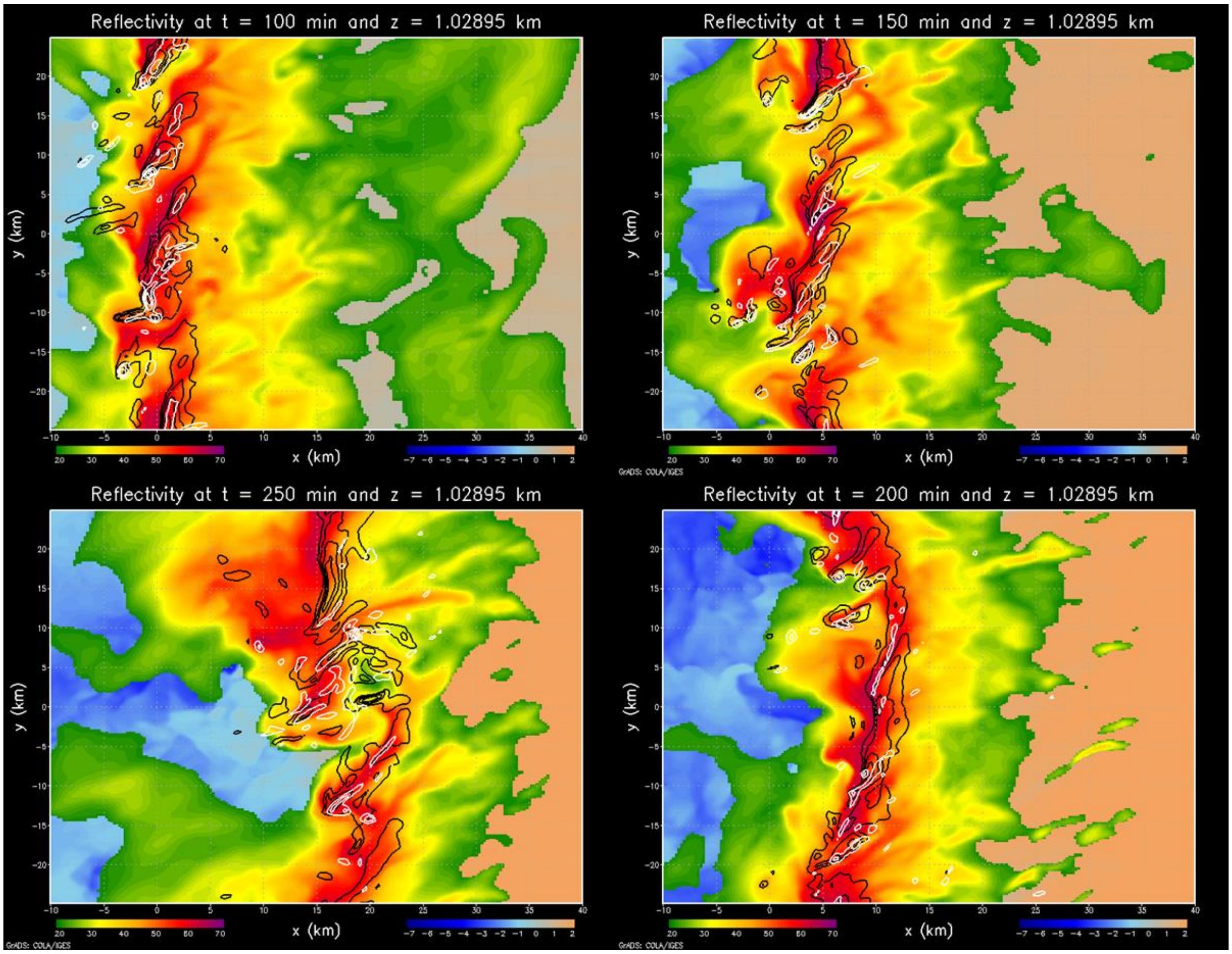

Figure 6. As in Fig. 4, but for ball cap CCW simulation.

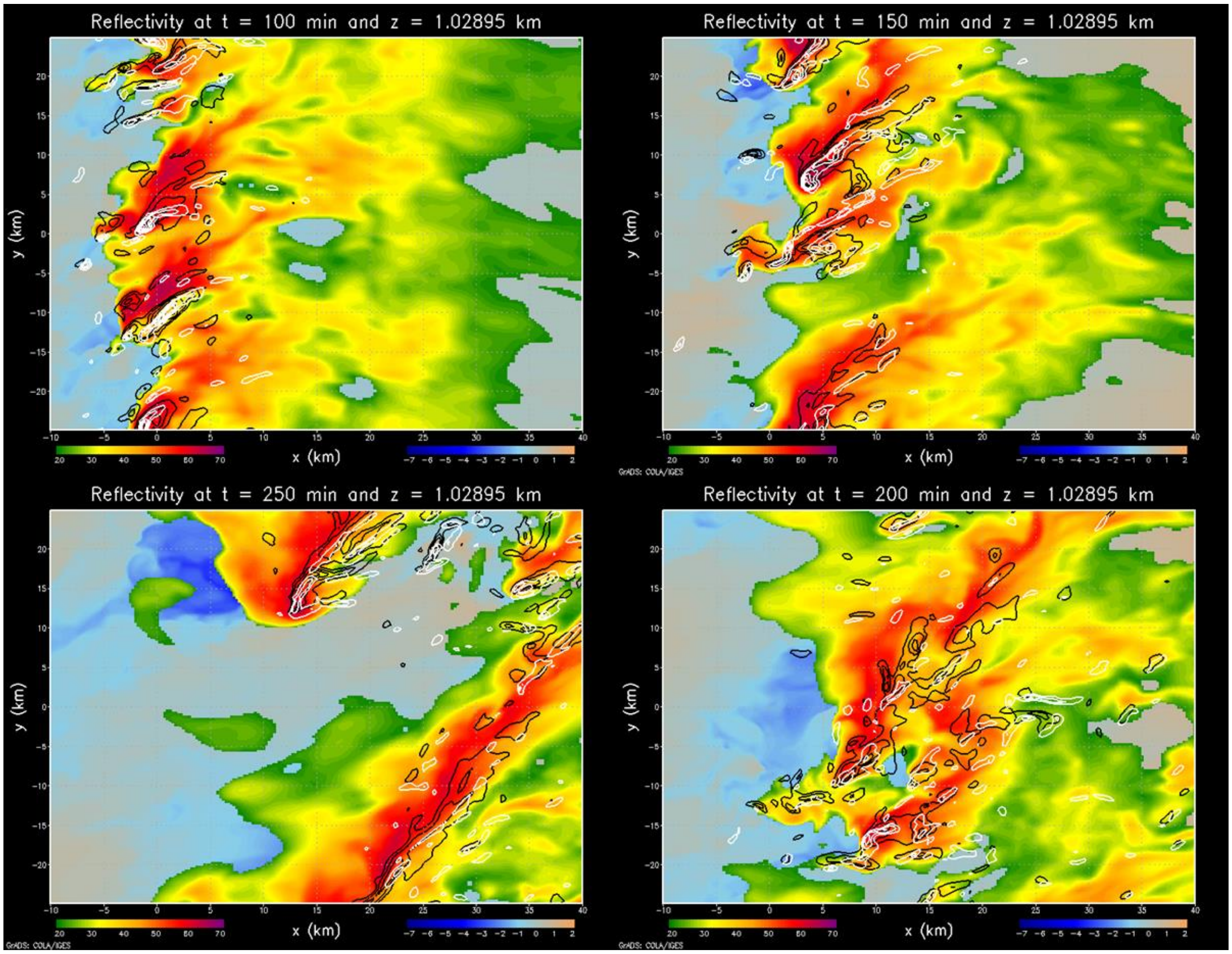

Figure 7. As in Fig. 4, but for quarter turn control simulation.

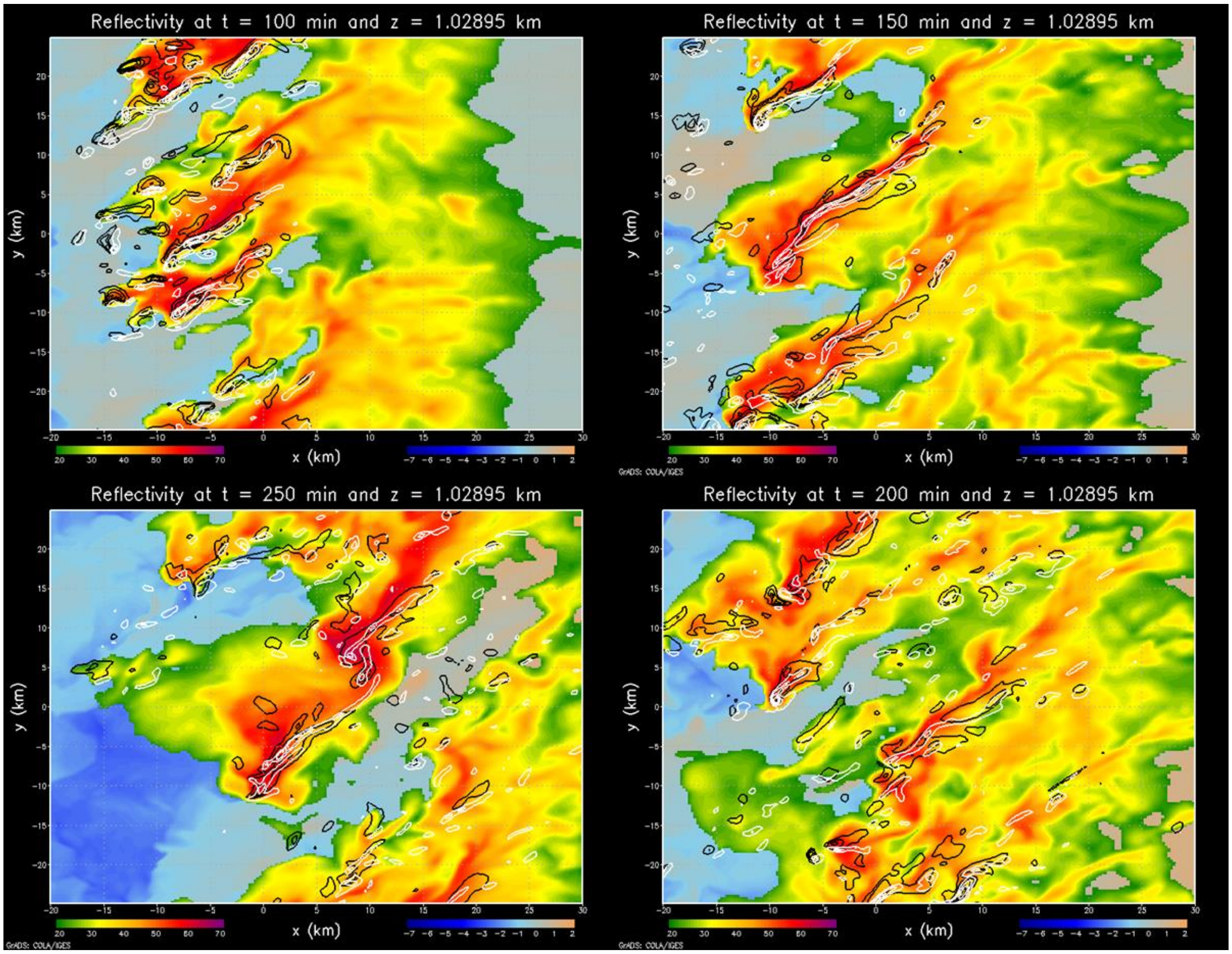

Figure 8. As in Fig. 4, but for spatula control simulation.

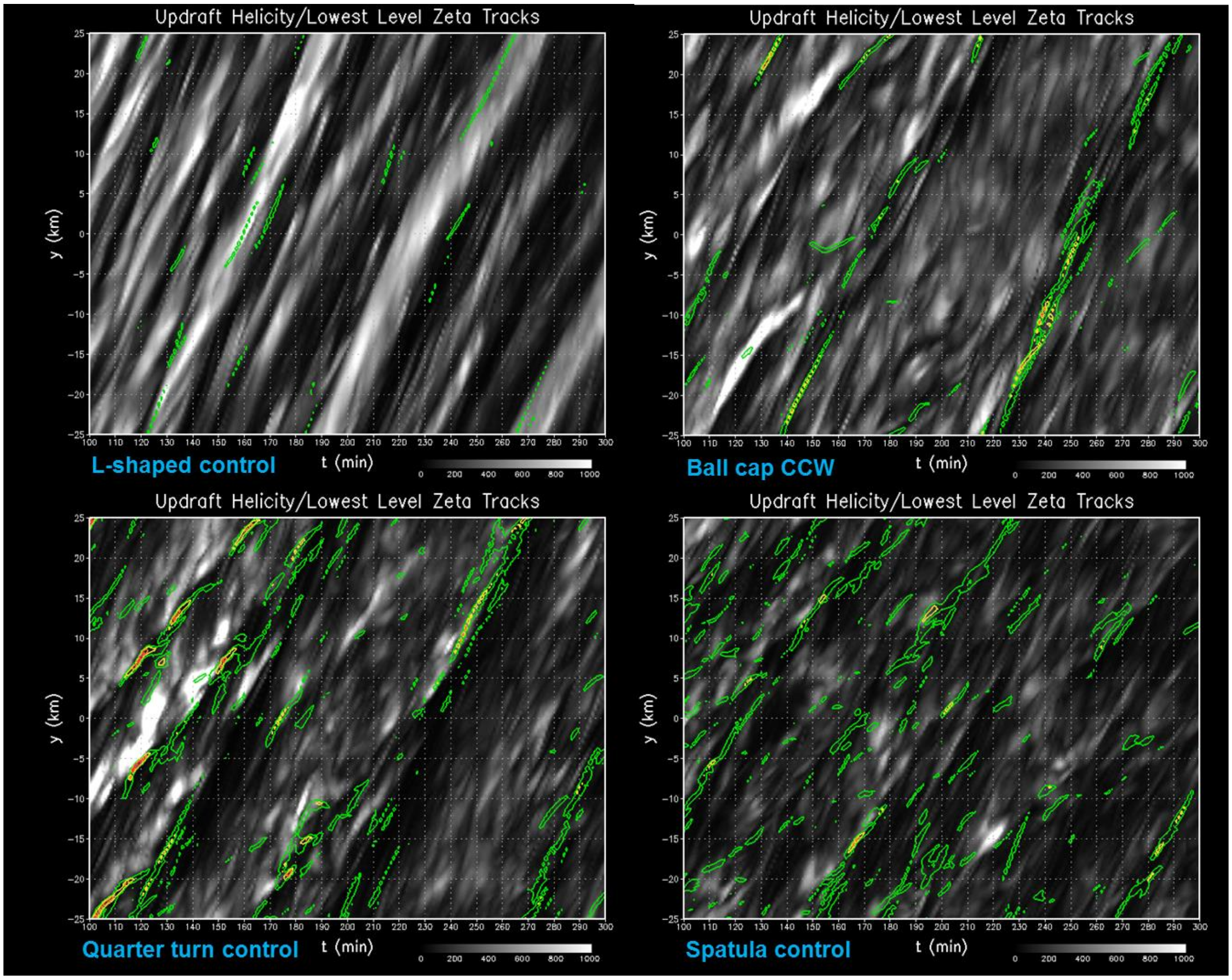

Figure 9. Hovmoller plots with simulation run time (min) on the abscissa and y (km) on the ordinate. Fields depicted are maximum updraft helicity ($m^2\ s^{-2}$, shaded in greyscale) and lowest-level vertical vorticity (green: 0.025 s^{-1}, yellow: 0.05 s^{-1}, orange: 0.075 s^{-1}, red: 0.1 s^{-1}, magenta: 0.15 s^{-1}) within the inner 100 km in the x-domain.

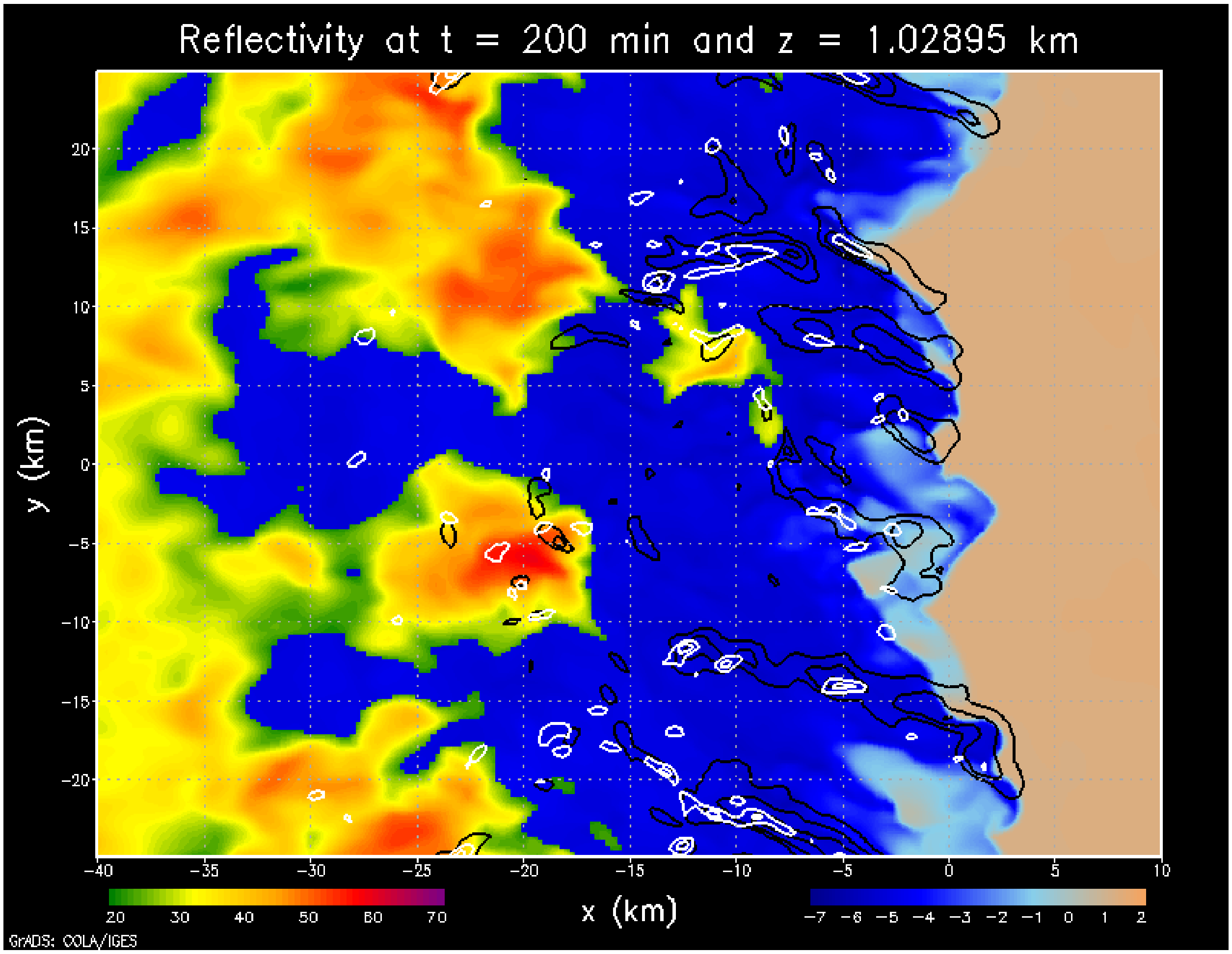

Figure 10. Example of overrunning convection from the quarter turn CCW simulation.

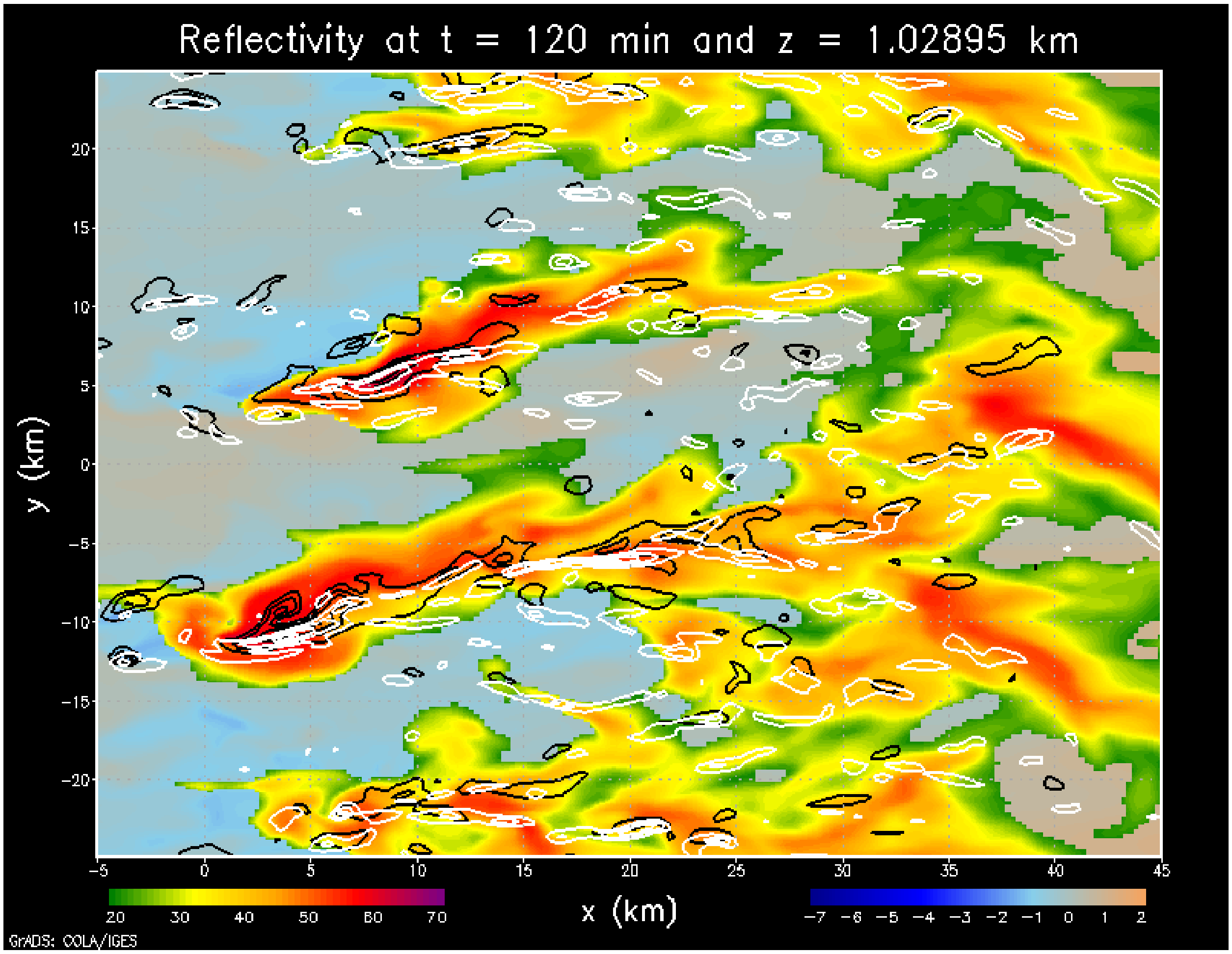

Figure 11. Example of shear-parallel convective bands from the ball cap control simulation.